A&A manuscript no.
(will be inserted by hand later)

Your thesaurus codes are:
missing; you have not inserted them

ASTRONOMY
AND
ASTROPHYSICS
13.2.1996

Observational limits on the contribution of sub-stellar and stellar objects to the galactic halo ⋆

R. Ansari[1], F. Cavalier[1], M. Moniez[1], E. Aubourg[2], P. Bareyre[2], S. Bréhin[2], M. Gros[2], M. Lachièze-Rey[2], B. Laurent[2], E. Lesquoy[2], C. Magneville[2], A. Milsztajn[2], L. Moscoso[2], F. Queinnec[2], C. Renault[2], J. Rich[2], M. Spiro[2], L. Vigroux[2], S. Zylberajch[2], J.-P. Beaulieu[3], R. Ferlet[3], Ph. Grison[3], A. Vidal-Madjar[3], J. Guibert[4], O. Moreau[4], F. Tajahmady[4], E. Maurice[5], L. Prévôt[5], C. Gry[6],

[1] Laboratoire de l'Accélérateur Linéaire, IN2P3-CNRS, Université de Paris-Sud, Centre d'Orsay, F-91405 Orsay Cedex, France
[2] CEA, DSM, DAPNIA, Centre d'Etudes de Saclay, F-91191 Gif-Sur-Yvette, France
[3] Institut d'Astrophysique de Paris, 98 bis Boulevard Arago, F-75014 Paris, France
[4] Centre d'Analyse des Images de l'INSU, Observatoire de Paris, 61 avenue de l'Observatoire, F-75014 Paris, France
[5] Observatoire de Marseille, 2 place Le Verrier, F-13248 Marseille Cedex 04, France
[6] Laboratoire d'Astronomie Spatiale de Marseille, Traverse du Siphon, Les Trois Lucs, F-13120 Marseille, France

Received aa/bb/95, accepted xx/yy/95

Abstract. EROS (Expérience de Recherche d'Objets Sombres) has been monitoring the luminosity of 4 million stars in the Large Magellanic Cloud in order to search for gravitational microlensing by unseen objects in the galactic halo. We present here the results from 3 years of EROS Schmidt plates data. Two stars exhibit light curves that are consistent with a sizeable microlensing effect. CCD data obtained later on revealed that one of these stars is an eclipsing binary system. Combining Schmidt plates data and the published results from our 16 CCD camera, we set upper limits on the number of unseen objects in the halo in the mass range $[10^{-7}, 1]M_{\odot}$.

Key words: dark matter – Galaxy : stellar content ; halo – brown dwarfs – Magellanic Clouds – gravitational lensing –

1. Introduction

The study of rotation curves of spiral galaxies has led to the hypothesis of the presence of massive extended halos of "dark matter" (e.g. Primack *et al.* 1988). Numerous candidates have been proposed as constituents of this matter, such as weakly interacting massive particles (WIMPS), massive neutrinos, or "brown dwarf" stars, i.e. stellar bodies lighter than the thermonuclear ignition limit ($M < 0.07M_{\odot}$ to $0.1M_{\odot}$, depending on the metallicity) (Carr 1990). Their existence could more specifically solve the question of the missing *baryonic* mass, which emerged from primordial nucleosynthesis studies (e.g. Kolb & Turner 1990).

Paczyński (1986) pointed out the possibility of using the gravitational microlensing effect to detect such massive halo objects. Four teams, EROS (Aubourg *et al.* 1993a,b, 1995), MACHO (Alcock *et al.* 1993, 1995a,b), OGLE (Udalski *et al.* 1993, 1994a) and DUO (Alard *et al.* 1995a) are now searching for those effects on resolved light sources, EROS and MACHO having started with the search for the effect on LMC stars.

A halo object passing close enough to the line of sight of a star in the Large Magellanic Cloud (LMC), would temporarily magnify its light (microlensing effect). At a given time t the apparent light amplification is determined by

$$A(t) = \frac{u(t)^2 + 2}{u(t)\sqrt{u(t)^2 + 4}} \ , \qquad (1)$$

where $u(t)$ is the distance between the undeflected line of sight and the deflecting object, expressed in units of the "Einstein Radius"

$$R_E = \sqrt{\frac{4GM}{c^2} Lx(1-x)} \qquad (2)$$
$$\simeq 970 \times \sqrt{\frac{M}{M_{\odot}}} \times \sqrt{\frac{L}{10\ Kpc}} \times \frac{\sqrt{x(1-x)}}{0.5} \times R_{\odot} \ .$$

Here G is the gravitational constant, L is the distance to the source, xL is the distance to the deflector and

Send offprint requests to: M. Moniez; *see also our WWW server at URL* `http://www.lal.in2p3.fr/EROS/eros.html`

⋆ This work is based on observations made at the European Southern Observatory, La Silla, Chile.

M its mass. The motion of the deflector relative to the line of sight to the source makes the magnification vary with time: for deflectors of masses within the interval $[10^{-7}, 1]M_\odot$ located in the halo, time scales range typically from hours to months for a significant variation in the magnification of a source in the LMC. Assuming a deflector moving at a constant apparent transverse speed V_T, reaching its minimum distance to the undeflected line of sight (impact parameter) u_{min} at time t_0, $u(t)$ is given by $u(t) = \sqrt{u_{min}^2 + ((t-t_0)/\Delta t)^2}$.

The "lensing time scale" $\Delta t = \frac{R_E}{V_T}$ is the only measurable parameter bringing useful information about the deflector. For a source in the LMC ($L = 55kpc$), it can be expressed as:

$$\Delta t(days) = 91 \times \left[\frac{V_T}{200km/s}\right]^{-1} \times \left[\frac{M}{M_\odot}\right]^{\frac{1}{2}} \times \frac{[x(1-x)]^{\frac{1}{2}}}{0.5} \quad (3)$$

The probability for a given star of the LMC to be amplified by a factor larger than 1.34 ($u = 1$) at a given time, is the probability for its line of sight to intercept the Einstein disk of radius R_E of one of the deflectors. This probability, the optical depth τ, scales with the total mass of the halo. Details of the halo geometry fix the value of the proportionality coefficient.

The standard isothermal halo model we use assumes a total galactic mass of $4.10^{11}M_\odot$ within 50 kpc of the galactic centre, and a radial density $\rho(r)$ decreasing as :

$$\rho(r) = \rho_0 \times \frac{a^2}{r^2 + a^2} \quad (4)$$

where r is the distance to the galactic centre. We have taken $a = 7.8$ kpc for the core radius (Caldwell & Ostriker 1981). For this model, the optical depth τ is about 4.5×10^{-7} up to the LMC. The velocity distribution of the deflectors is assumed to be boltzmannian, with a dispersion of 245 km/s. Assuming that all deflectors have the same mass M, the rate per star for microlensing effects with amplifications greater than a threshold amplification A_T (corresponding to an impact parameter $u_{min} = u_T$) has been calculated to be $1.6\ 10^{-6}\ u_T\sqrt{M_\odot/M}\ yr^{-1}$ (De Rujula *et al.* 1991, Griest 1991).

The microlensing effect has some very characteristic features which should enable to discriminate it from any known intrinsic stellar variability :

- The event is singular in the history of the source (as well as of the deflector).
- The gravitational origin of the effect implies that the magnification is independent of the colour.
- The luminosity is a known function of time, depending on only 3 parameters $(u_{min}, t_0, \Delta t)$, with a symmetrical shape.

The latter two characteristics are affected if there is a deviation from the approximations of a single point-like deflector and source and of uniform motion (see section 6). In addition, statistical tests may be applied to a set of microlensed stars :

- As the geometric configuration of the source-deflector system is random, the impact parameters of the events have to be uniformly distributed. This allows the prediction of the theoretical amplification distribution which, corrected for microlensing detection efficiency, can be compared with the observed one.
- The passive role of the lensed stars implies that their population should be representative of the monitored sample, particularly with respect to colour and magnitude.

2. The observations

To fully cover the range of possible microlensing time scales, EROS has performed two observing programs, one using a 16 CCD camera mounted on a 40 cm diameter telescope (Arnaud *et al.* 1994, Aubourg *et al.* 1995), to search for short time scale microlensing phenomena, and the other using Schmidt photographic plates. We present here results from the latter program, superseding our previous publication (Aubourg *et al.* 1993b).

During 3 annual periods of about 6 months, 290 usable photographic plates (in total) of 29×29 cm^2 have been exposed at the E.S.O Schmidt telescope (1 meter free aperture, f/3). Half of the plates (098-04 emulsion) were taken with a RG630 red filter and half (IIaO emulsion) with a GG385 blue filter. Exposure times were 1 hour in each colour, and apart from the very crowded LMC bar region, our star detection efficiency abruptly drops at a limiting magnitude of around 20.5 in red and 21.5 in blue. The data taking period is limited by the maximum excursion of the telescope around the meridian position ($\pm$2.5 hours). The time sampling of the plates (see figure 1), makes the ex-

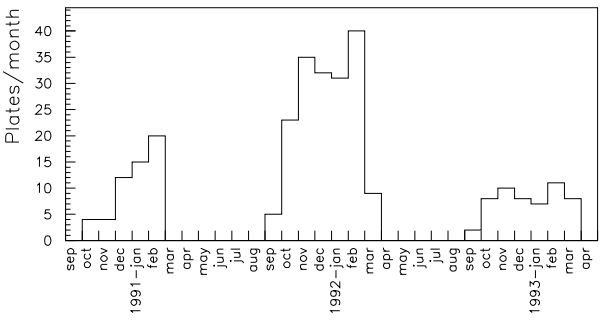

Fig. 1. *Time distribution of the photographic plates taken for EROS (from 1990 to 1993).*

periment sensitive to microlensing event durations ranging from a few days to a few months. Two thirds of the plates were taken during the second year, and the first period was irregularly sampled. The seeing, comprised in the interval [0.9, 2.] arcsec has an average value of about 1.5 arcsec. The scale of the images is 67.5 arcsec/mm and the usable field covered with a plate is $5.2^\circ \times 5.2^\circ$, centered on position ($\alpha = 5h20mn, \delta = -68^\circ 30'$) (eq. 2000). The transmission coefficient T of each plate was digitized to 0.8 giga-pixels (12 bits) of 10 microns size (0.675 arcsec) using the "MAMA"[1] microdensitometer (Machine Automatique à Mesurer pour l'Astronomie) at the Observatoire de Paris (Berger *et al.* 1991). The digitization takes 6 hours per plate.

3. Data reduction

We have divided the field into 28x28 sub-fields of 1cm^2 each, and have checked that the response of a plate digitized by the "MAMA" measuring machine does not significantly vary at the centimeter scale. Each stage of the following analysis is then performed locally for each subfield. A home-made photometric program has been developed, optimised for the search for variations in crowded fields, which have an occupation rate of about 100 reconstructed stars/arcmin^2. A detailed description of the analysis can be found in Aubourg (1992), Cavalier (1994), Laurent (1995).

3.1. From pixels to light curves

The quantity $\Phi_T = [(1-T)/T]^{0.6}$ varies approximately linearly with the flux Φ collected on the photographic plate in the magnitude range [17, 21] (blue) [16, 20] (red). We therefore use Φ_T in our photometric fitting and starfinding procedures. The thus obtained star magnitudes are then corrected using an empirical formula providing an accuracy of 0.2 magnitude in average, which is derived from comparison of selected fields with CCD measurements taken with the E.S.O-Danish 1.54m telescope. As a check of the validity of this empirical formula over the whole plate field, we have measured that the mean magnitude and magnitude dispersion of the red giant clump are constant within 0.07 mag for each 1cm^2 sub-field where those numbers can be correctly estimated, i.e. outside the LMC bar.

The first step of the reduction was to construct a reference catalogue of stars for each colour, using a composite image obtained by adding 10 aligned and resampled images, taken under good conditions. From such a composite image, the detection of stars is improved due to the better signal/noise ratio. Their positions are measured with a better accuracy than on a single image, allowing to use these as reference positions. Their luminosities are also used as reference ones. We have detected 8 million stars in at least one colour, while 6 million are seen in the two colours.

Each 1 cm^2 sub-field of each digitized plate is then submitted to the following treatment, leading to new luminosity measurements for each catalogued star :

- The geometrical correspondence between a current image and the reference catalogue is determined with a positioning precision better than $2.5\mu m$ (0.17 arcsec) using a pattern recognition program, which associates the brightest stars detected by a crude algorithm, with the brightest stars of the reference catalogue.
- The point spread function (PSF) of a star centered at position $\boldsymbol{r_0}$ is described by a Moffat Function (Moffat 1969) $\Phi(\boldsymbol{r}) = A \times (1 + \frac{|\boldsymbol{r}-\boldsymbol{r_0}|^2}{\sigma^2})^{-3}$. From a sample of well defined and well isolated stars, we determine the parameter σ of this PSF, which we have found to be approximately independent of the flux of the stars (except for those which saturate the plate, or are underexposed).
- Using the geometrical transformation, the position of each catalogued star is predicted on the current image, and the luminosity of the stars are measured by fitting only one parameter per star (the amplitude A of the PSF, centered on the predicted position). This procedure is considerably faster, and also more precise, than fitting simultaneously the positions *and* the fluxes of each star. To extract the flux of the stars in a crowded environment, the amplitudes of all the stars and a common background within a 0.5×0.5mm^2 sliding window with 0.3mm step are fitted together, and only the measurements of the stars in the 0.3×0.3mm^2 central part are retained.
- The incoming fluxes on the plates depend on observational conditions such as atmospheric transmission, seeing or exact exposure time. In particular, measured luminosities are affected by the seeing in a way that depends on the environment of the stars, due to the imperfect knowledge of the PSF and to the limits of validity of the procedure. We correct for the differences in the data taking conditions by requiring that the mean luminosity of stars in a given luminosity interval and for a given estimated background due to neighbouring stars be equal to their mean reference luminosity.

A file, one for each colour, containing the time series of luminosity measurements (hereafter light curve) is then updated with these corrected values for each star. The uncertainty σ_i on a luminosity measurement Φ_i depends mainly on the luminosity of the star and on the global quality of image number i, determined by the seeing and the sky background. For each 1cm^2 sub-field of each plate i, we determine empirically the resolution σ_i as a function of the luminosity, by comparing the star fluxes Φ_i with their reference values to estimate standard deviations. A detailed description of the parametrisation of σ_i can be found with our atlas of LMC stars (Aubourg *et al.* 1996).

[1] MAMA is developed and operated by INSU/CNRS.

The performance of this reconstruction procedure is summarized in figure 2, which shows the mean dispersion of the measurements along the light curves as a function of the magnitude m_B (and m_R) in the EROS blue (red) filter band, for stars having at least 90 reliable measurements for each colour.

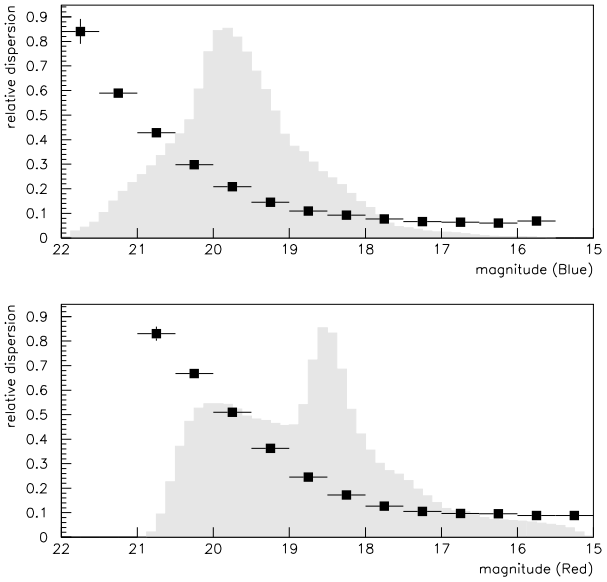

Fig. 2. *Relative plate to plate average dispersion of the luminosity measurements versus magnitude (upper= EROS blue, lower= EROS red). This dispersion is taken as an estimator of the photometric precision. The superimposed hatched histograms show the magnitude distribution of the stars.*

3.2. Analysis of the light curves

The next step of the analysis is to test each light curve for the presence of a microlensing event. Algorithms to be applied to the light curves to search for microlensing candidates should accept light curves exhibiting one and only one positive fluctuation that is greater than that expected from measurement errors. Additionally, the magnifications in the two colours should be equal within errors and the temporal development of the magnification consistent with the one expected from a microlensing effect.

Two independent analyses using different approaches have been developed in order to select the microlensing candidates. The first one was intended to extract a clear and isolated signal, with a high signal/background ratio appropriate to our ignorance of the risk of false events. It uses criteria based on the expected shape of a microlensing effect, which are relevant only for sufficiently sampled events. The other analysis includes the search for undersampled events, with a higher detection efficiency for events of a few days. It does not take into account the shape of the light variation and uses criteria mainly based on fluctuation probabilities. The efficiency of each of the following criteria to accept real microlensing events has been studied and optimised with Monte-Carlo generated lensing light curves (section 5).

3.2.1. First analysis of the light curves

This analysis (Cavalier 1994) starts from a sample of 4.2 million stars with reliable measurements in both colours. Given this large number of light curves, we define a reduced sample using a crude selection filter to remove stable stars which did not exhibit any significant fluctuation. We adjust the filtering in order to select about 10% of the light curves.

Each light curve from this prefiltered set (0.44 million stars) is then subjected to a series of tests to select microlensing events:

- We first require the existence of a bump (i.e. at least 3 consecutive measurements above the base flux by more than 1.2σ) in both colours, each having its maximum flux within the duration of the other.
- Then we compute the correlation coefficient of the blue and red luminosity variations during the bumps, and require this coefficient to be larger than a given threshold, such as to reject the 40% objects with the most chromatic fluctuations.
- In order to have well defined base fluxes for stability studies, we limit the duration of the bump to a maximum of 100 days. At this stage of the analysis, 7140 stars are selected.
- Then we fit the observed light curves with a theoretical microlensing function defined for each colour λ as the product of the amplification function $A(t)$ by a constant base flux F_λ. Parameters u_{min} (linked to the maximum amplification A_{max} through eq. (1)), t_0, Δt and F_λ are adjusted independently for each colour using least-squares fits. A global fit is also performed on the whole set of measurements, constraining the function A(t) to be the same for the two colours.
  This fitting procedure provides reliable fitted parameters t_0 and Δt for 707 pairs of light curves, the other ones mostly showing erratic variations.

Figure 3a shows the distribution of the red magnitudes for these 707 stars. This distribution is dominated by the brightest stars, amongst which the fraction of variable stars is high.

Two sets of rejection criteria concerning independent measurements are finally used :

- The first one combines a test of shape and a loose achromaticity requirement using only the measurements taken *during* the bump. To test for the shape,

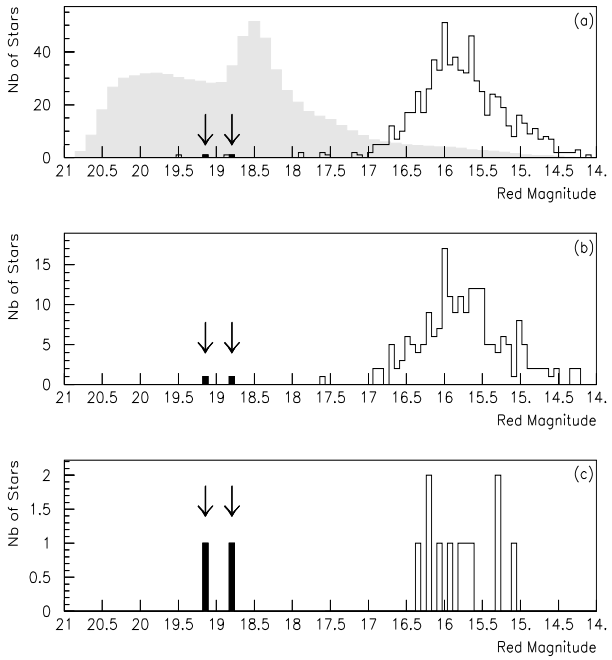

Fig. 3. *Magnitude m_R of selected stars at various stages of the first analysis*
(a) : before applying the last two sets of tests. The grey histogram shows the shape of the distribution for the unbiased initial sample of 4.2 million stars.
(b) : after requiring the shape and achromaticity criteria.
(c) : after requiring the stability of the star outside the bump. The two marked events are the only ones surviving all the tests.

we require the χ^2 of the global fit mentioned above to be less than 2.5/d.o.f. For testing achromaticity, we require the χ^2 obtained by fitting the red measurements imposing the $A(t)$ function adjusted in blue, to be less than 4/d.o.f. (loose test). 206 stars survive this set of tests. If we consider that this sample is still dominated by a background of classical types of stars (stable or variable), the rejection power of the set is $707/206 \simeq 3.4$.

– The second set of rejection criteria tests the stability of the light curve *outside* the bump. We first require the correlation between the blue and red light curves to be weak outside this bump, and therefore compatible with random measurement errors. We also require the calculated probability of the most important fluctuation with respect to a constant flux found outside the main bump to be more than 10^{-9} for both colours. 13 stars out of 707 survive this set of tests, which then has a rejection power of $707/13 \simeq 54$.

Figure 3b (c) shows the distribution of the red magnitudes for stars which satisfy the first (second) set of tests. Only the 2 stars with the magnitudes marked with an arrow on figure 3 satisfy both sets of tests.

3.2.2. Background

The 707 stars with significant structures of bumps are mainly variable stars lying within the instability strip and the red giant branch. Except for the two selected stars, they exhibit either obviously periodic variabilities or a main chromatic or asymmetrical bump with other smaller variations. A few may also be intrinsically stable stars with groups of deviating measurements. For this mixture of stars, the global rejection of the last two sets of tests should be larger than the product $3.4 \times 54 = 186$, because they are anti-correlated: if a significant bumpy structure is found, then the probability for the corresponding star to be a true variable having other significant variations outside this bump is higher than for stars which do not satisfy the first set of tests. In the sub-sample of stars with R magnitude larger than 17 we find that less than 0.13 star from the above mixture are expected to accidentally survive the selection process, and be considered as microlensing-like events. In this statistical calculation, only the variable types effectively present in the sample of 707 stars can be accounted for, and it is not possible to estimate the contamination due to some other rare type of variable star. Anyway, we should consider such contamination as a "signal" in the sense that, using our data only, there is no way to distinguish it from a real microlensing effect.

3.2.3. Second analysis of the light curves

This analysis, described in detail in (Laurent 1995), is restricted to the 3.33 million best measured stars, located at least 3 mm away from the outer edges of the analysed region (the 28×28 1cm^2 sub-fields), well isolated and with magnitudes within or close to the linear regime, and whose light curves are correctly sampled in both colours during all three seasons. Twenty five plates showing abnormally large seeing or response dispersions or non-circular star images are excluded from the analysis. Each light curve is then subjected to the following selection process.

A search for the first and second most significant fluctuations is done for each colour, using the probability of the χ^2 of successive measurements with respect to the base flux (the base flux is defined as the average flux in the two seasons where the star luminosity is lowest). Each selected fluctuation should contain at least 3 measurements more than 0.5 σ from the base flux and one measurement more than 2.0 σ from the base flux. In addition, the first fluctuation is required to correspond to a luminosity increase. We do not allow fluctuations to span more than one season (see figure 1).

- We require that light curves exhibit significant first fluctuations in both colours, with a modest (at least 8 %) time overlap, leaving 6912 stars.
- We then require the second fluctuation to have both a low absolute significance and a low significance relative to the first one. The aim here is to reject most periodic variable stars, except those with periods larger than a year or smaller than a few days.
- In the remaining sample of only 44 stars, 34 exhibit long time scale fluctuations (at least two thirds of a season) with slow luminosity variation. These stars, most of which are bright, are removed by requiring that the dispersion of the luminosity measurements be significantly higher during the season of the first (main) fluctuation than during the other two seasons. This criterium rejects long-period variable stars.
- We then require that the correlation coefficient between the blue and red light curves outside the main fluctuations be compatible with zero at the 4 standard deviation level. This test rejects three short period variable stars.
- From the 7 remaining stars, only 4 pass a loose achromaticity test (compatibility of the variations for the 2 colours within 5 standard deviations).
- We found that 2 of those 4 stars are located 4 arcsec apart and are contaminated by a nova (IAU circular 5651). They passed the selection process because there is no criterion based on the shape of the variations. The other 2 light curves are the same as found in the first analysis.

The fact that the two different selection processes isolate *the same two light curves* reinforces their status as peculiar events, whatever their final interpretation.

4. Complementary observations

We started detailed observations on the two candidates to further check their validity as possible microlensed stars.

Old plates have been examined to check the constancy of the fluxes on a time scale of a few years. High resolution imagery has been taken at the E.S.O New Technology Telescope. We found no pathologic feature (like the presence of bright nearby stars). No anomaly appears from UBVRI photometry of the two candidates. The two stars have been found to lie within the LMC from spectral measurements (Beaulieu *et al.* 1995). They are also from two distinct stellar types (see table 1): EROS #1 candidate is a B star with H emission lines, that may indicate the presence of surrounding gas, and EROS #2 is an A star.

To test for any further variability, photometric measurements have been made using our 16 CCD camera, mounted on a 40 cm diameter telescope (Arnaud *et al.* 1994). Some photometric measurements were also provided by the 70 cm Geneva telescope at E.S.O. in La Silla. Data concerning the candidates have also been extracted from a series of plates exposed in 1994 for our experiment. Finally, the EROS #2 candidate has benefitted of a specific treatment which allowed us to recover a total of 142 measurements from the 1990-93 plates ; as the star lies close to the edge of the plates, its neighbourhood is truncated and despite the fact that the star is present on each plate, the pattern recognition phase of the geometrical alignment procedure, which needs the neighbouring stars, had failed in a large number of cases.

From the new CCD measurements, we discovered that EROS #2 is an eclipsing binary star with period 2.8169 ± 0.0005 days, and amplitude at the 0.5 magnitude level (Ansari *et al.* 1995). More measurements are needed to elucidate the nature of the single high amplitude bump we detected.

5. Calculation of the microlensing detection efficiency

To determine the efficiency of each rejection criterium, we have applied them to Monte-Carlo generated light curves of microlensing events. We have developed two independent simulation programs of the microlensing effect, using different ways to take into account the imperfectly known photometric uncertainties.

The first program generates light curves through the following procedure: the base fluxes of a lensed star in the two colours are randomly chosen following the observed magnitude versus colour distribution of catalogued stars. Then we calculate the lensing effect due to the crossing of an object of fixed mass (10^{-5} to $1 M_{\odot}$), at impact parameter u_{min} in the interval $[0, 2]$, with distance to the Earth and speed spanning the standard halo model (Caldwell & Ostriker 1981). The time of maximum amplification t_0 was picked at random in a 3 year period containing all photographic plates of figure 1. Then a light curve is generated, with our experimental time sampling, and with random gaussian shifts corresponding to the uncertainties measured from the data for such luminosities.

The other program starts from the observed light curves, and superimposes the effect of an amplification from a microlensing on the measured values, to produce new light curves and error bars. Microlensing light curves were simulated with time scales Δt in the range $[0.3, 600]$ days, and with the same u_{min} and t_0 parameters distributions than in the first program.

The light curves produced by the two simulation programs have been submitted to the selection programs, to provide us with an expected number of events in the hypothesis of a halo made of equal mass objects. For a given analysis, the two programs give compatible estimates.

Figure 4 shows the detection efficiency for the second analysis, normalized to the microlensing events with impact parameter $u_{min} \leq 1$, as a function of the time scale Δt of the microlensing effect. Figure 7a (curve labelled "Plates") shows the expected number of events in the sec-

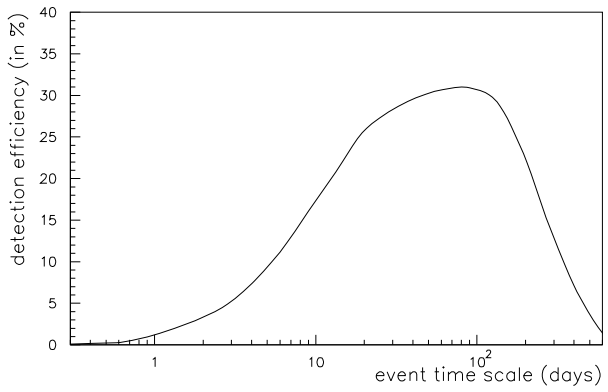

Fig. 4. *EROS Schmidt plates microlensing detection efficiency* $\epsilon(\Delta t)$ *as a function of event time scale* Δt*, from our second analysis.*
$\epsilon(\Delta t)$ *is the ratio of the number of detected events with any* u_{min} *to the number of events generated over a full 3 year period, with* $u_{min} \leq 1$*. This efficiency is independent of the halo model.*

ond analysis as a function of the mass of the deflectors, assuming a delta distribution for the halo object masses.

6. Study of systematic uncertainties

6.1. Uncertainties from the simulation programs

The two simulation programs give compatible estimates within 5% when used to calculate the detection efficiency of a given selection program. The difference can be explained by the different photometric error modeling. This 5% is taken as the systematic uncertainty for the detection efficiency that is associated with our imperfect knowledge of the resolution.

The simulation programs also use the generated amplifications as measured amplifications thus assuming that the plates are correctly calibrated. The magnitudes have been empirically derived by comparison with CCD images (see section 3.1), but the slope of the calibration line cannot be obtained with a precision better than 5 percent. This induces a 5 percent uncertainty in the expected number of events.

6.2. The single source approximation

The efficiency calculations described above assume that the light curves represent the light from only one star so that the entire flux would be microlensed in an event. In fact, a large proportion of stars are in binary systems and the microlensing light curve may be distorted because of different amplifications for the two components. However, this would affect our detection efficiency only if the two stars are of comparable magnitude and have a projected separation in the deflector's plane larger than half the Einstein radius. The fraction of such pairs is sufficiently small that the effect on our efficiency calculation should be negligible (Griest & Hu 1992).

On the other hand, in crowded fields one must consider the possibility that stars are accidentally "blended" so that a light curve receives significant contributions from two or more stars whose images overlap. This effect can be studied by reconstructing artificially produced images of known star content. Previous studies have shown an efficiency reduction of $\sim$ 20% for the MACHO collaboration survey of the central regions of the LMC (Alcock *et al.* 1995b) and $\sim$ 10% for the EROS CCD survey of the LMC bar (Aubourg *et al.* 1995). We expect a smaller effect for the present study because of the smaller density of stars studied (1.2 10^5 resolved stars per square degree) compared to MACHO (9.5 10^5 stars per square degree) and EROS CCD (1.9 10^5 stars per square degree). Additionally, the fact that we reconstruct most of the red giant clump stars means that there are fewer stars just below detection threshold compared to the EROS CCD study where the threshold was near the middle of the clump.

Studies with Monte Carlo fabricated images (Laurent 1995) have confirmed that this effect of blended stars is small, contributing an error of less than 10 percent to the expected number of events. We include this as part of our systematic error.

6.3. The point-like source approximation

The efficiency calculations also assume that the sources are point-like objects. This approximation breaks down when the size of the star projected onto the plane of the deflector is comparable to the impact parameter. For the deflector masses studied here, this can only affect very high amplification events and has no effect on our detection efficiency.

6.4. The single lens approximation

A small fraction of the deflectors are expected to be multiple systems giving more complex microlensing light curves ; a few percent of the observed microlensing light curves do display such features (Udalski *et al.* 1994b, Alard *et al.* 1995b). Anyhow the second analysis, which do not require a specific shape for the light curves, is able to detect them, except in the rare cases where two peaks are clearly separated. The detection efficiency, calculated under the assumption of single lenses, should then not be significantly affected.

6.5. Loss of efficiency from subsequent requirements

The use of the subsequent CCD observations to test the two candidates for more criteria (see section 4) could in principle reduce the detection efficiency.

We estimate that less than 1% of the monitored stars do not lie in the LMC, and must be subtracted from the number of sources used to calculate our detection efficiency. This can be considered as a negligible effect.

We have also checked that in the fields specially monitored with the camera, a negligible fraction of stars do exhibit fluctuations larger or equivalent to the fluctuations of EROS #2. This means that if we could systematically perform the same complementary observations that were done for the two candidates, and remove sources with variability at a level comparable to EROS #2, we would reject a negligible fraction of microlensing targets.

6.6. Uncertainties from the Halo model

We have investigated the sensitivity of the expected number of microlensing events to the values of the parameters in the Halo model, keeping the total mass within 50 kpc at $4.10^{11} M_{\odot}$. The core radius has been varied between 3 and 8 kpc ; the distance of the Sun to the Galactic centre has been varied by 0.5 kpc ; the average velocity of halo objects was varied by 10 % ; we have allowed for the uncertainty in the LMC velocity. Adding all the resulting changes in number of events in quadrature, one finds a typical error from these parameter uncertainties of 15 %. Flattening the Halo along the Galactic pole axis by up to a factor of three decreases the expected number of events by at most 10 %. We have also used the Halo model parameters of Griest (1991) ; they correspond to expected number of microlensing events typically 15 % higher than those given here (figure 7a).

7. Discussion

7.1. Microlensing fits and statistical features

Figures 5 and 6 show the light curves of the two selected stars with the fitted microlensing curves, on a truncated time scale. The fit of a microlensing effect is superimposed onto the modulation found with our complementary observations for the EROS #2 candidate (see Ansari *et al.* 1995 for details). Separate fits were first calculated for both colours and were found compatible within errors, allowing us to use combined fits. This feature of the light curves, together with the good χ^2 values, make them compatible with a microlensing effect. Table 1 gives the relevant fitted parameters for the two candidates.

The two candidates have spatial locations and magnitudes which are typical in our monitored sample. The maximum magnifications we have observed would correspond to lens configurations with reasonable probabilities (impact parameters respectively 0.44 and 0.40 Einstein radius).

Table 1. Characteristics of the two microlensing candidates

	EROS #1	EROS #2
Coordinates of star (eq. 2000)	$\alpha = 5h26m34.1s$ $\delta = -70°57'45"$	$\alpha = 5h06m05.2s$ $\delta = -65°58'33"$
m_B	19.4 ± 0.2	19.2 ± 0.2
m_R	18.9 ± 0.2	19.1 ± 0.2
Type of star	B6-7 Ve or IVe	A0-2 V
Radial velocity	$350 \pm 170 km/s$	$300 \pm 155 km/s$
Date of maximum amplification	1 Feb. 1992	29 Dec. 1990
Event time scale R_E/V_T (in days)	23 ± 2	29 ± 2
Max. amplification (in magnitudes)	1.0 ± 0.1	1.1 ± 0.1
Impact parameter (in Einstein radius)	0.44 ± 0.02	0.40 ± 0.03
χ^2 of combined fit	131/279 d.o.f.	154/273 d.o.f.
Remarks		binary system period 2.8 days

Given the unusual natures of our candidates, to be conservative, we have for now to consider them either as possible unusual types of variable stars or as microlensing events. This means that when establishing statistical upper limits on the standard halo mass from our observations, we consider that we have observed 2 or less microlensing events.

7.2. Constraints on the galactic halo

We discuss now consequences of our observations in an increasing order of model-dependence.

7.2.1. Signal

Taking into account the maximum statistical contamination of 0.13 event expected from the known types of variable stars (section 3.2.2.), we find that the probability to find one event or more from those known origins is 12%, and the probability to find two or more events is only 0.8%.

The contribution of the LMC to the optical depth along our line of sight has been discussed by Gould (1993 & 1994) and Sahu (1994). We have computed the number of microlensing effects from LMC non dark matter (i.e. excluding haloes), using the ratio of LMC-disk to Galactic halo event rates from Wu (1994) and our expected event rate for the Galactic halo. We thus estimate the expected

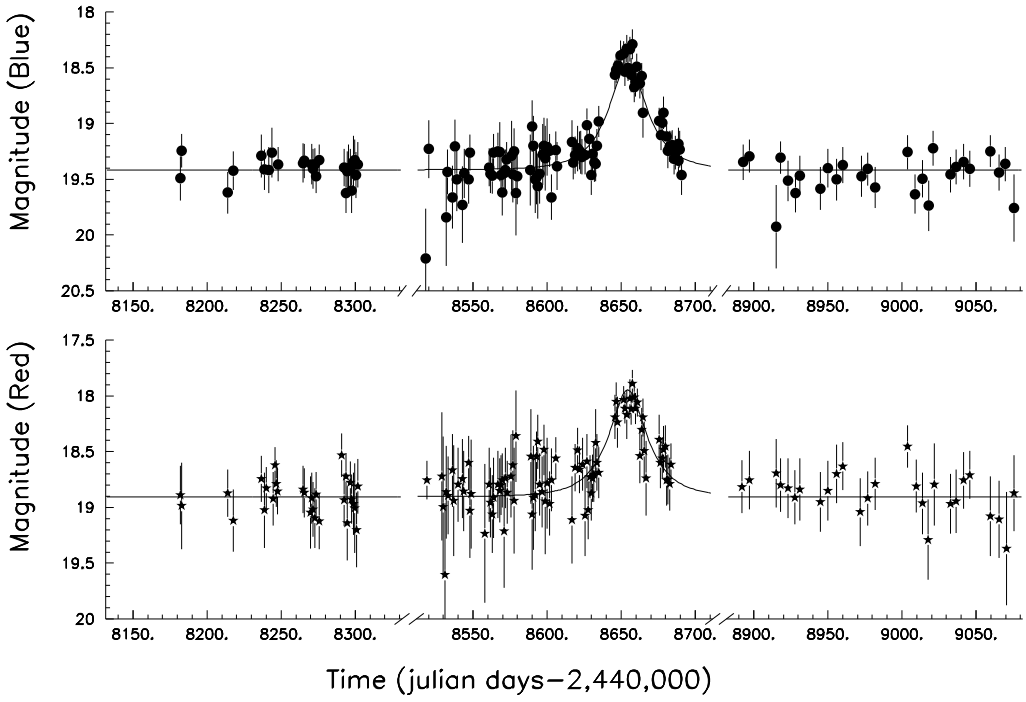

Fig. 5. *Light curves of the EROS #1 candidate. Data recorded with the blue (red) filter are presented in the upper (lower) figure. One should note the non-continuous horizontal axes : the three parts correspond respectively to data recorded in 1991, 1992 and 1993. Microlensing curves calculated with the global fitting procedure of the first analysis are superimposed on both light curves.*

number of microlensing events from deflecting stars located in the LMC disk itself to be less than 0.6. One should notice that the fact that our candidates lie far from the LMC bar makes more unlikely the possibility of lensing by LMC stars. We have also estimated the microlensing events expected from stars in the Galactic disk to be less than 0.15.

7.2.2. Optical depth and event rate

The optical depth, given by the fraction of time during which a star undergoes a lensing amplification larger than 1.34, is computed from

$$\tau = \frac{\pi}{2.E} \sum_{events} \frac{\Delta t}{\epsilon(\Delta t)}$$

where $E = 3.33\ 10^6 stars \times 3\ years = 1.0\ 10^7 star \times year$ is our exposure for the second analysis and $\epsilon(\Delta t)$ the detection efficiency for this analysis as a function of Δt, normalized to the lensing events with $u_{min} \leq 1$ and to a full 3 year period (fig. 4). If we assume that our two candidates are due to real microlensing effects, then the corresponding detected optical depth is $8.2\ 10^{-8}$.

The event rate is computed to be $\Gamma = 1/E \times \Sigma_{events}(1/\epsilon(\Delta t)) = 7.3\ 10^{-7} events/star/year$.

7.2.3. Masses of the deflectors

For given time scales Δt of 23 and 29 days, we have computed, for all possible masses, the probability to pick a microlensing event due to a halo object with duration Δt, or a less probable one. Mass intervals where this probability is higher than 5% are $[0.01-0.7]M_\odot$ (resp. $[0.02-1.1]M_\odot$) for $\Delta t = 23$ (resp. 29) days.

7.2.4. Limits on the composition of the galactic halo

Figure 7a, established using the Monte-Carlo simulation, shows the number of events expected to be selected by the second analysis, for the standard halo described in section 1, assuming that all lenses have the same mass. This distribution is plotted for the presently described EROS Schmidt plates data and also for the EROS CCD experiment (Aubourg *et al.* 1995), the results of which are almost completely independent because of the different sets of monitored stars and time samplings. Adding in quadrature all the systematic uncertainties discussed in sections 6.1 to 6.5, one gets a 15% global systematic uncertainty on the number of events expected in the EROS Schmidt plates experiment. As discussed in section 6.6, excursions of the halo parameters compatible with the standard model contribute an additional 15% uncertainty on the expected number of events.

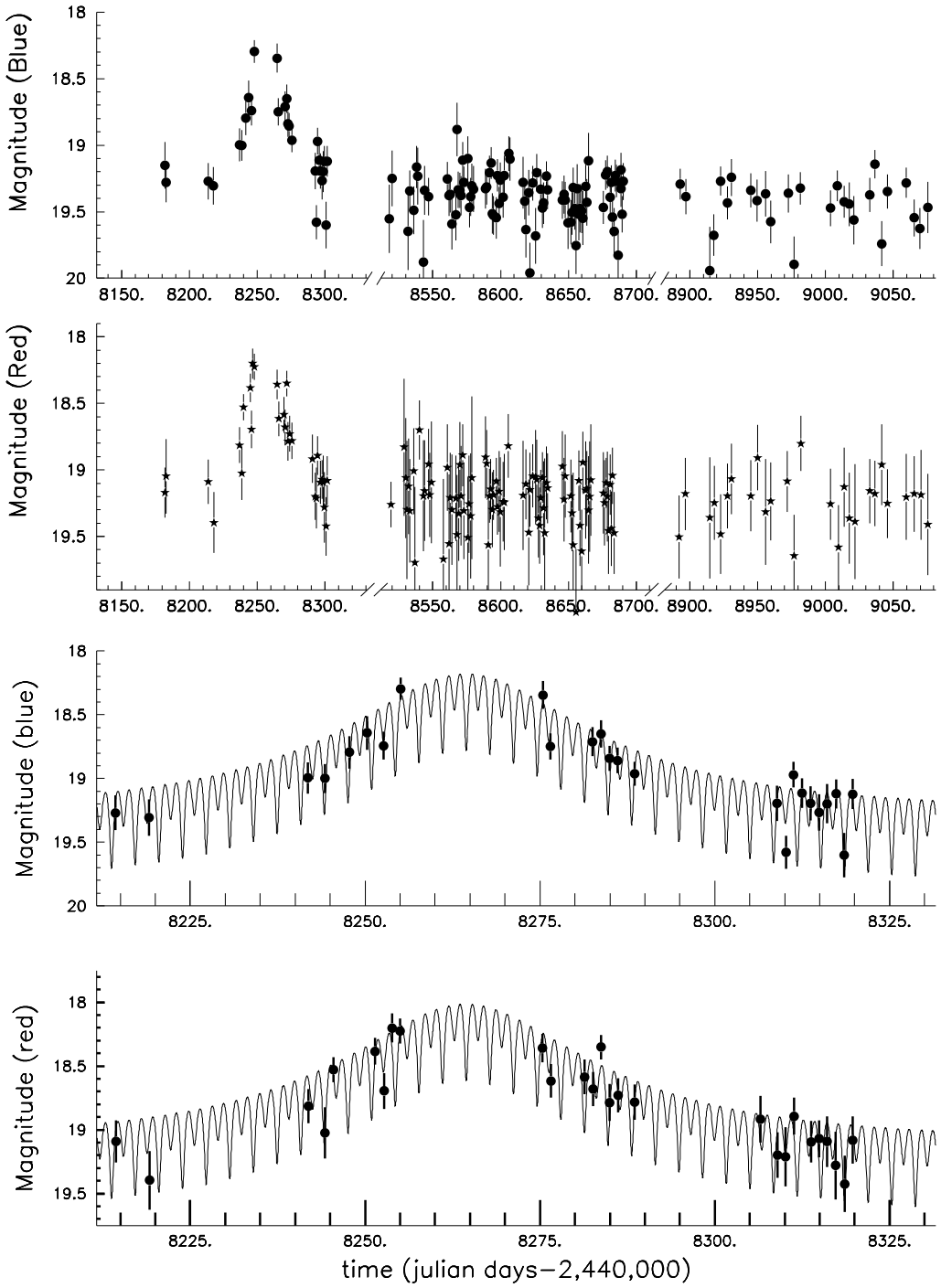

Fig. 6. *Light curves of the EROS #2 candidate. On the lower part, the fit of the function of a microlensing variation combined with the periodic variability of the eclipsing system is superimposed on the 1991 data points.*

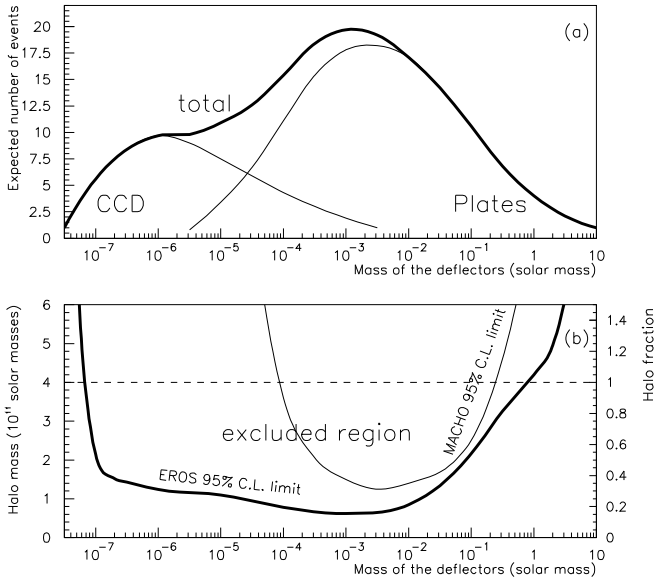

Fig. 7.
(a) : number of events expected to satisfy the requirements of the analysis, assuming all deflectors have the mass given in abscissa, in the Schmidt plates data (second analysis), in the CCD data, and in total.
(b) : the excluded contribution at, 95% confidence level, of massive objects to the standard spherical halo, expressed in mass within 50 kpc (left scale) and in standard halo fraction (right scale), assuming a delta distribution for the mass of the deflectors. The excluded region at 95% C.L. from the MACHO experiment is also drawn (Alcock et al. 1995a, b).

Figure 7b gives the maximum contribution of massive objects to the standard halo compatible with our observations at 95% confidence level, as a function of their mass (obtained for the case of delta function mass distributions). We establish this exclusion contour making use of the combined sensitivities of the two EROS experiments and taking into account the time scales of the two detected events (23 and 29 days) in a simple and conservative way ; from the estimated number and Δt distribution of the events expected with given mass deflectors, we compute the fraction of the standard halo for which the probability to find 0, 1 or 2 events in the $[13, 52]$ days time scale interval, multiplied by the probability to find 0 event outside this interval, is lower than 5%.

From the two EROS experiments, we conclude that at 95% C.L., objects of masses in the interval $[10^{-7}, 10^{-1}]M_{\odot}$ cannot contribute more than 50% to the mass of the standard halo, and objects of masses in the interval $[3.10^{-5}, 10^{-2}]M_{\odot}$ cannot contribute more than 25%.

The most probable halo fraction and deflector mass published by the MACHO collaboration (Alcock *et al.* 1995a) are obviously not excluded by our results.

The results presented here are to a large extent independent of the results of the MACHO collaboration (Alcock *et al.* 1995a) also shown on fig 7b, because 80% of the EROS measurements were made before MACHO data taking and the sets of monitored stars have a small intersection, due to the chosen fields and different limiting magnitudes.

We stress that our sensitivity is not large enough to put constraints on the galactic dark matter distribution if it exhibits a geometrical shape significantly different from the standard halo model. This would be for example the case of a thick disk or a strongly flattened halo (more than a factor of 8). We plan to discuss constraints for such alternative models in a separate paper (in preparation).

8. Conclusion

We have searched for microlensing events with durations ranging from a few days to a few months. Using two independent analysis, we found two events which could be interpreted as microlensing events due to objects with probable masses between 10^{-2} and $1M_{\odot}$ if they lie in the galactic halo. One of the two selected stars was later found to be an eclipsing binary system, and cannot be considered as a reliable candidate. It is anyway not possible to rule out the possibility of having detected new types of irregular variable stars, and we expect to improve our knowledge about the two candidates from various observations. Combining the results presented here from the Schmidt plates experiment, and earlier ones from our CCD experiment, allows us to put significant constraints on the contribution of massive compact objects to the mass of the standard galactic halo.

Acknowledgements. We thank A. Bijaoui for discussions, G. and O. Pizarro for taking the photographic material, and the MAMA team, particularly R. Chesnel and P. Toupet for their participation to plate scanning.

References

Alcock C., Akerlof C.W., Allsman R.A. et al. 1993, Nat 365, 621
Alcock C., Allsman R.A., Axelrod T.S. et al. 1995a, Phys. Rev. Lett. 74 , 2867
Alcock C., Allsman R.A., Axelrod T.S. et al. 1995b, submitted to ApJ
Alard C., Guibert J., Bienayme O. et al. 1995a, *Messenger 80, 31*
Alard C., Mao S. & Guibert J. 1995b, A&A 300, L17-L20
Ansari R., Cavalier F., Couchot F. et al. 1995, A&A 299, L21
Arnaud M., Aubourg E., Bareyre P. et al. 1994, Exp. Ast., 4, 265 (I) & 279 (II)
Aubourg E. 1992, Ph.D. thesis, report DAPNIA/SPP 92-22

Aubourg E., Bareyre P., Bréhin S. et al. 1993a, *Messenger* 72, 20
Aubourg E., Bareyre P., Bréhin S. et al. 1993b, Nat 365, 623
Aubourg E., Bareyre P., Bréhin S. et al. 1995, A&A 301, 1
Aubourg E., Bareyre P., Bréhin S. et al. 1996, *in preparation*
Beaulieu J.P., Ferlet R., Grison P. et al. 1995, A&A 299, 168
Berger J., Cordoni J.P., Fringant A.M. et al. 1991, A&AS 87, 389
Caldwell, J.A.R. & Ostriker, J.P. 1981, ApJ 251, 61
Carr, B.J. 1990, Comments Astrophys. 14, 257
Cavalier, F. 1994, Ph.D. thesis, report LAL 94-18
De Rujula, A. et al. 1991, Mont. Not. R. Astr. Soc. 250,348
Gould, A. 1993, ApJ 404, 451
Gould, A. 1994, ApJ 421, L71
Griest, K. 1991, ApJ 366, 412
Griest, K. & Hu, W. 1992, ApJ. 397, 362
Kolb, E. W. & Turner, M. S. 1990, The Early Universe, Addison-Wesley
Laurent, B. 1995, Ph.D. thesis, report DAPNIA/SPP 95-1002
Moffat, A.F.J. 1969, A&A 3, 455
Paczyński, B. 1986, ApJ 304, 1
Primack, J. Seckel, D. & Sadoulet, B. 1988, Ann. Rev. Nuc. Part. Sci., B38, 751
Sahu, K.C. 1994, Nat 370, 275
Udalski A., Szymański M., Kaluzny J. et al. 1993, Act. Astr. 43, 289
Udalski A., Szymański M., Stanek K.Z. et al. 1994a, Act. Astr. 44, 165
Udalski A., Szymański M., Mao S. et al. 1994b, ApJ 436, L103
Wu, X.P. 1994, ApJ 435, 66

This article was processed by the author using Springer-Verlag LaTeX A&A style file *L-AA* version 3.